Dissociation Dynamics of N_2O in Superexcited States As Probed by Two-Dimensional Fluorescence Spectroscopy

Shuntaro Machida,[†] Masatoshi Ukai,[‡] Masashi Kitajima,[†,§] Kosei Kameta,[†] Noriyuki Kouchi,[†] Yoshihiko Hatano,*[,†] Tatsuji Hayaishi,[||] and Kenji Ito[⊥]

Department of Chemistry, Tokyo Institute of Technology, Meguro-ku, Tokyo 152, Japan, Department of Applied Physics, Tokyo University of Agriculture and Technology, Koganei-shi, Tokyo 184, Japan, Institute of Applied Physics, University of Tsukuba, Tsukuba, Ibaraki 305, Japan, and Photon Factory, National Laboratory for High Energy Physics, Tsukuba, Ibaraki 305, Japan

Received: July 8, 1996; In Final Form: October 4, 1996[⊗]

The dispersed fluorescence yields of excited photodissociation fragments of N_2O are obtained by means of the two-dimensional fluorescence spectroscopy as a function of both the excitation energy (E_{ex}) in the range 14.28−36.35 eV and the fluorescence wavelength (λ_{fl}) in the range 80−200 nm. Final dissociation products, dissociation limits, and correlation among different neutral dissociation channels are identified. In most cases of the neutral dissociation of superexcited states below 20 eV, neutral dissociation is shown to proceed via multichannel predissociation. The $nd\pi$ Rydberg states converging to $N_2O^+(C^2\Sigma^+)$ are shown to have the neutral dissociation channel with specific branching ratios for their decay. The neutral dissociation into $N_2(a^1\Pi_g)$ + O is shown to diminish at the threshold energy for the three-body neutral dissociation. Broad features of enhanced fluorescence above 20 eV are identified as multiply excited neutral states.

1. Introduction

Primary and secondary processes following photoabsorption of molecules in the extreme-ultraviolet region are strongly influenced by superexcited states, i.e., the neutral states above the first ionization threshold of the molecule. Among various decay processes of molecular superexcited states, the dissociation, especially neutral dissociation, in competition with the autoionization has been shown to play an important role in the extreme-ultraviolet photophysics and photochemistry above ionization thresholds.[1,2] The difficulties of detecting neutral products, however, hampered the experimental investigation of neutral dissociation. Thus, in the region far beyond the ionization threshold, most of the experimental studies have been restricted to those of photoionization and the measurements of photoabsorption spectra. However, since they are not so sensitive to superexcitation owing to a huge contribution from direct ionization, most of superexcited states, especially those having repulsive potential curves or surfaces, have not yet been revealed. The observation of neutral dissociation of simple molecules by detecting undispersed fluorescence from excited fragments using optical filters has been shown to be a useful tool for studying the decay of superexcited states.[3−5] Such fluorescence originates from the neutral dissociation of molecular superexcited states. This fluorescence technique has made it possible to get the information on repulsive potential structures of molecular superexcited states as well as on well-defined vibrational levels of bound superexcited states. However, since most of the investigations through fluorescence observation have been carried out by measuring yields of undispersed fluorescence, they have not provided detailed information on particular dissociation products and precise dissociation limits, which is indispensable for understanding the dissociation and autoionization dynamics of superexcited states. The yields of dispersed fluorescence have been recently measured to study the dissociation dynamics of superexcited states of O_2[6] and CO[7] by means of the two-dimensional fluorescence spectroscopy.

In the present experiment, the yields of dispersed vacuum ultraviolet fluorescence from excited fragments produced by excitation of N_2O are measured as a function of the excitation photon energy (E_{ex}) for the following processes, e.g.,

$$N_2O + h\nu(E_{ex}) \rightarrow O^* + N_2 \quad (1)$$

$$O^* \rightarrow O + h\nu'(\lambda_{fl}) \quad (2)$$

Nitrous oxide, N_2O, has been extensively studied previously through photoabsorption,[8,9] photoionization,[10−14] ion pair formation,[15,16] and high-energy electron scattering[17−19] experiments, providing energy levels and the autoionization behavior of superexcited states. The photoionization quantum yield,[9] i.e., the ratio of the photoionization cross section to the total photoabsorption cross section, has shown many vibrational and broad structures above the first ionization threshold, which has made the photoionization quantum yield less than unity. From these results a possibility of the significant role of the neutral dissociation of superexcited N_2O has been pointed out. Only a few studies on the neutral dissociation of superexcited states, however, have so far been reported.[5,20,21,22] Guyon et al.[22] suggested that the neutral dissociation path should play an important role in a process competing with the autoionization of superexcited N_2O ejecting zero kinetic energy electrons, i.e., autoionization should be influenced by neutral dissociation. The investigation of neutral dissociation is therefore helpful for a better understanding of the autoionization.

The purpose of the present work is to understand in more detail the superexcited states of N_2O and their dissociation dynamics by observing the final dissociation products over a

* To whom all correspondence should be addressed. E-mail: yhatano@chem.titech.ac.jp.
[†] Tokyo Institute of Technology.
[‡] Tokyo University of Agriculture and Technology.
[§] Present address: The Institute of Physical and Chemical Research (RIKEN), Wako-shi, Saitama 351-01, Japan.
[||] University of Tsukuba.
[⊥] National Laboratory for High Energy Physics.
[⊗] Abstract published in *Advance ACS Abstracts,* December 15, 1996.

S1089-5639(96)02017-8 CCC: $14.00

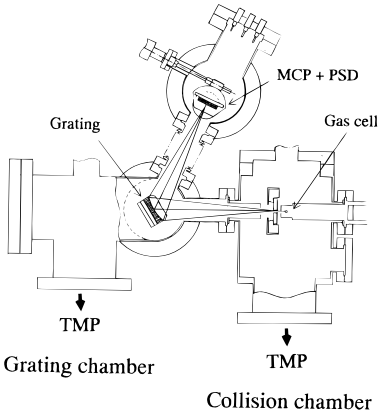

Figure 1. Experimental apparatus. The right side is a collision chamber, and the left side is a monochromator to disperse the fluorescence resulting from excitation by monochromatized synchrotron radiation focused into a gas cell perpendicular to this figure.

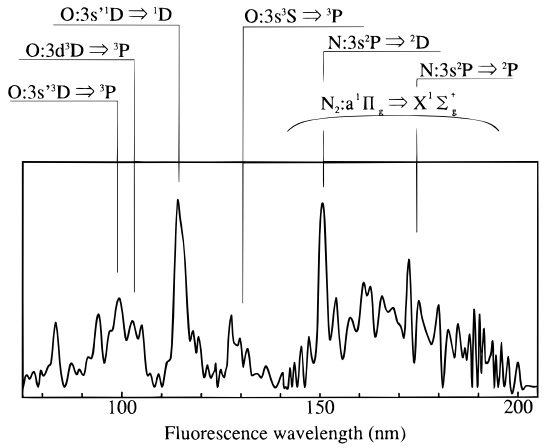

Figure 2. Fluorescence spectrum in the photodissociation of N_2O at a photon energy of 16.02 eV.

wide range of excitation energy. The dispersed fluorescence yields are obtained as a two-dimensional fluorescence excitation spectrum (2D-FES) where the yields are plotted as a function of both excitation photon energy and fluorescence wavelength.[6,7]

The fundamental properties for N_2O are as follows. The ground-state configuration of N_2O without the three K shells is $(4\sigma)^2(5\sigma)^2(6\sigma)^2(1\pi)^4(7\sigma)^2(2\pi)^4$ or $X^1\Sigma^+$.[23,24] Vertical ionization potentials for one-electron ionic states are 12.89 eV for $(2\pi^{-1})$ $X^2\Pi$, 16.38 eV for $(7\sigma^{-1})$ $A^2\Sigma^+$, 18.23 eV for $(1\pi^{-1})$ $B^2\Pi$, and 20.11 eV for $(6\sigma^{-1})$ $C^2\Sigma^+$.[9] Moreover, some ionic satellites are known in the region of the present excitation energy[17] of which the threshold energies are 24 eV for MET-I, 28.5 eV for MET-II and 33 eV for MET-III.[17] In this paper we use the abbreviated term "MET" standing for the multiple electron transition state of ion for such satellites as named and numbered in ref 17.

2. Experiment

The experiment was performed at the Photon Factory in Tsukuba. Synchrotron radiation (SR) from a 2.5 GeV positron storage ring was monochromatized with a 3 m normal incidence monochromator.[25] The typical band-pass was 0.26 nm. Figure 1 shows the outline of the secondary monochromator, which consists of a collision chamber and a grating chamber. The monochromatized SR was focused into a gas cell that contained N_2O gas. Vacuum ultraviolet fluorescence was dispersed by the secondary monochromator equipped with a holographic 1200 lines/mm grating with a curvature radius of 20 cm at a dispersion angle of 64°. A fluorescence spectrum was recorded using a resistive anode-type position sensitive detector (PSD) behind a microchannel plate (MCP) coated with CsI.[6,7,26] The photon detection efficiency by the present MCP−PSD combination is known to be a smoothly decreasing function of the fluorescence wavelength from 80 to 200 nm. Because of the weak fluorescence intensity, we employed a 2 nm band-pass for the secondary monochromator. The primary photon flux was monitored by a combination of a sodium salicylate scintillator and a photomultiplier (PMT) behind the gas cell. During the experiment, the gas pressure was kept constant at about 40 mTorr and monitored by a capacitance manometer. Fluorescence spectra were obtained in the range of the excitation photon wavelength of 34.1−86.8 nm for the fluorescence wavelength range 80−140 nm and in the range of the excitation photon wavelength of 34.1−85.1 nm for the fluorescence wavelength range 140−200 nm with an interval of 0.1 nm. The yields were normalized for the primary photon flux and the N_2O pressure but not corrected for the efficiency of the whole fluorescence detection system.

3. Results

Figure 2 shows a fluorescence spectrum of N_2O at the excitation photon energy of 16.02 eV, where many fluorescence lines are shown. They are emitted by excited atomic and molecular fragments produced in the photodissociation of N_2O, and some of them are assigned as shown in Figure 2. The broad structure in the fluorescence wavelength of 150−200 nm is due to the molecular fluorescence of the $N_2(a^1\Pi_g)$ fragment. Because of the low resolution of the secondary monochromator, some fluorescence lines overlap with others.

Figure 3 shows a gray scale plot of the 2D-FES surface. Each rectangular dot represents the yield of dispersed fluorescence in exponentially increasing order from light to dark with 20 degrees of gradation. Ionization potentials for some of the one-electron ionic states are also indicated in Figure 3. The fluorescence spectrum shown in Figure 2 corresponds to the horizontal cross-sectional view of the 2D-FES at the excitation photon energy of 16.02 eV. Diagonal structures in the 2D-FES are due to scattered primary light, which appear at higher order positions of the secondary monochromator.

Despite the low resolution of the fluorescence wavelength and small fluorescence yields, many atomic fluorescence lines are assigned more easily with the visual enhancement of the resolution in the 2D-FES. For example, it is difficult to assign the origin of fluorescence at 130.4 nm unambiguously to O($3s^3S \rightarrow {}^3P$) or to find the trace of the N($3s^2P \rightarrow {}^2P$) fluorescence at 174.5 nm in Figure 2, whereas they are clearly seen in Figure 3 as "vertical lines" on the 2D surface despite many overlaps. It is no longer difficult to observe a lot of "vertical lines" of fluorescence from excited O and N atoms in Figure 3, which are identified and assigned with the lower levels in the transitions in O and N at the top of the 2D-FES. Some of fluorescence lines, however, could not be assigned unambiguously owing to the closely spaced transitions. The identified lines[27] are listed in Table 1 with the lowest threshold energies of neutral dissociation in producing fluorescent fragments.[28] Most of the atomic fluorescences show up in the 2D-FES when the excitation photon energy reaches their lowest threshold energies.

From the 2D-FES, one can unambiguously identify the origin of fluorescence lines as neutral dissociation in the region of the excitation photon energy below the lowest threshold energy of the dissociative ionization excitation (DIE) resulting in the emission of vacuum ultraviolet radiation detectable in the present experiment, i.e., 23.89 eV corresponding to the process $N_2O \rightarrow N_2(a^1\Pi_g) + O^+(^4S) + e^-$, where this threshold energy is the

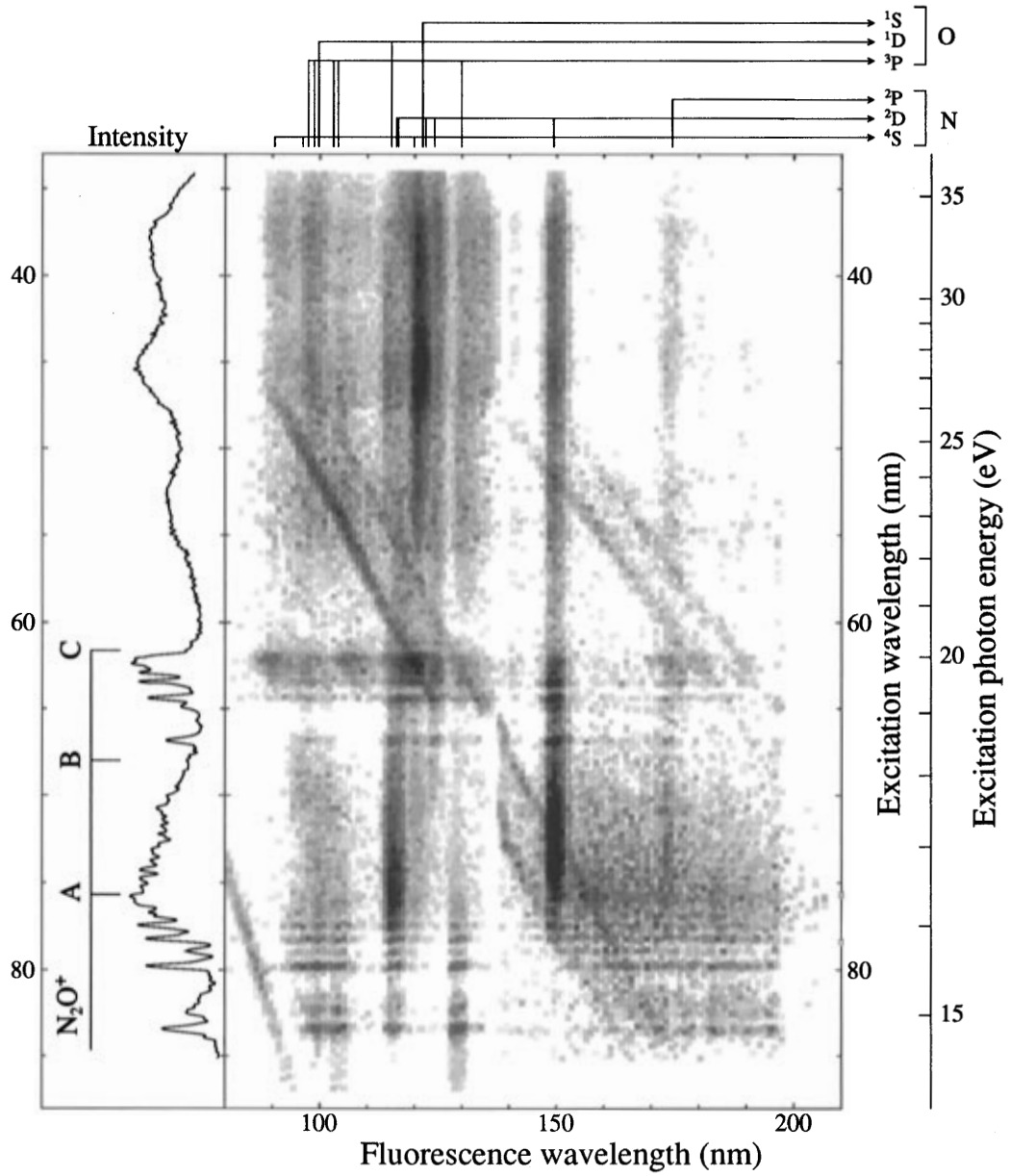

Figure 3. Two-dimensional fluorescence excitation spectrum (2D-FES) is divided into two parts. One is a spectrum as a function of both the excitation photon energy in the range 14.28−36.35 eV and the fluorescence in the range 80−140 nm. The other is a spectrum as a function of both the excitation photon energy in the range 14.57−36.35 eV and the fluorescence wavelength in the range 140−200 nm. The fluorescence intensity in the 2D-FES increases exponentially from light to dark. The total fluorescence yield curve is also shown in the left portion of the figure, of which intensity is on a linear scale. The positions of the fluorescence lines are indicated at the top of the figure.

sum of the bond dissociation energy of N_2−O, 1.68 eV, the internal energy of $N_2(a^1\Pi_g)$, 8.59 eV, and the lowest ionization energy of the ground-state O atom, 13.62 eV.[28]

The dependence of the fluorescence lines on the excitation photon energy is characteristic for each line, which gives rise to a drastic alteration of the fluorescence pattern in Figure 3. For example, the strong line at 115.2 nm from $O(3s'^1D)$ and that at 149.3 nm from $N(3s^2P)$ are seen in the region of the excitation photon energies lower than 20 eV, whereas the fluorescence line at 120.0 nm from $N(3s^4P)$ becomes strongest above 20 eV. Such behavior indicates the alteration of dissociation channels with the variation of excitation photon energy, which is due to the excitation to a particular superexcited state and the subsequent neutral dissociation leading to a particular dissociation limit(s).

An enhanced broad structure in the lower right corner on the 2D-FES in Figure 3 is due to the molecular fluorescence from N_2 fragments ($a^1\Pi_g \rightarrow X^1\Sigma_g^+$). No other pronounced molecular fluorescence is observed in the present experiment.

The total fluorescence yield obtained by summing the partial fluorescence yields over the fluorescence wavelengths of 80−200 nm at each excitation photon energy is presented in the left-hand portion of Figure 3. The present total fluorescence yield curve is generally similar to the undispersed FES measured in the range of the fluorescence wavelength of 113−180 nm and in the range of the excitation energy of 11.17−41.33 eV (see Figure 1 in ref 5). This agreement is understandable, since the fluorescence in the ranges 80−110 and 180−200 nm gives a small contribution to the total fluorescence yield as seen on the 2D-FES surface in Figure 3. In detail, however, a small difference between them in the relative intensities among the observed peaks is seen, which is due to the difference in detection efficiencies. The partial yields for several intense fluorescence lines are shown in parts a−f of Figure 4. Figure 4a shows the total fluorescence yield as mentioned above. Parts b−d of Figure 4 show the fluorescence yields of $N(3s^2P \rightarrow {}^2D)$, $O(3s'^1D \rightarrow {}^1D)$, and $O(3s^3S \rightarrow {}^3P)$, respectively. Parts e and f

TABLE 1: Fluorescent Fragments, Transitions, Fluorescence Wavelengths, Lowest Dissociation Processes for the Fragments, and Corresponding Threshold Energies Lower than 20 eV[a]

fragment	transition	fluorescence wavelength [nm]	lowest dissociation process	threshold energy [eV]
$O(3s'^3D)$	$3s'^3D \rightarrow {}^3P$	98.8	$O(3s'^3D) + N_2(X^1\Sigma_g^+)$	14.23
$O(3s''^1P)$	$3s''^1P \rightarrow {}^1D$	99.9	$O(3s''^1P) + N_2(X^1\Sigma_g^+)$	16.05
$O(3d^3D)$	$3d^3D \rightarrow {}^3P$	102.7	$O(3d^3D) + N_2(X^1\Sigma_g^+)$	13.75
$O(4s^3S)$	$4s^3S \rightarrow {}^3P$	104.1	$O(4s^3S) + N_2(X^1\Sigma_g^+)$	13.59
$O(3s'^1D)$	$3s'^1D \rightarrow {}^1D$	115.2	$O(3s'^1D) + N_2(X^1\Sigma_g^+)$	14.41
$N(3s^4P)$	$3s^4P \rightarrow {}^4S$	120.0	$N(3s^4P) + NO(X^2\Pi)$	15.26
$O(3s''^1P)$	$3s''^1P \rightarrow {}^1S$	121.8	$O(3s''^1P) + N_2(X^1\Sigma_g^+)$	16.05
$N(3s'^2D)$	$3s'^2D \rightarrow {}^2D$	124.3	$N(3s'^2D) + NO(X^2\Pi)$	17.29
$O(3s^3S)$	$3s^3S \rightarrow {}^3P$	130.4	$O(3s^3S) + N_2(X^1\Sigma_g^+)$	11.18
$N(3s'^2D)$	$3s'^2D \rightarrow {}^2P$	141.1	$N(3s'^2D) + NO(X^2\Pi)$	17.29
$N_2(a^1\Pi_g)$	$a^1\Pi_g \rightarrow X^1\Sigma_g^+$	LBH band	$N_2(a^1\Pi_g) + O(^3P)$	10.27
$N(3s^2P)$	$3s^2P \rightarrow {}^2D$	149.3	$N(3s^2P) + NO(X^2\Pi)$	15.62
$N(3s^2P)$	$3s^2P \rightarrow {}^2P$	174.5	$N(3s^2P) + NO(X^2\Pi)$	15.62

[a] Transitions are identified according to ref 27. Threshold energies are calculated with the constants in refs 27 and 28.

of Figure 4 show the partial yields for fluorescence in the ranges 95−105 and 118−122 nm, respectively.

The total fluorescence yield curve shows many sharp peaks, almost all of which are ascribed to the Rydberg states series converging to the one-electron ionic states as seen in Figure 4a. At these photon energies the partial yields of the fluorescence in parts b−f of Figure 4 are simultaneously enhanced, which appear as discrete "horizontal features" on the 2D-FES in Figure 3. This shows that Rydberg states interact with other neutral states causing a multistep predissociation among a number of potential surfaces (i.e., they dissociate into various dissociation channels). On the other hand, it is seen that a broad continuum overlaps with the peaks of the Rydberg states. This is noticeable in Figure 4b for $N(3s^2P \rightarrow {}^2D$ at 149.3 nm) and in Figure 4c for $O(3s'^1D \rightarrow {}^1D$ at 115.2 nm) in the range of the excitation photon energy of 16−18 eV (see also Discussion section B.2 below). Those features correspond to the excitation to the repulsive superexcited N_2O states followed by dissociation down the repulsive potential surfaces. In the range of the excitation photon energy higher than 20 eV only broad structures of enhanced fluorescence yields are recorded on the 2D-FES surface in Figure 3 corresponding again to the dissociation down the repulsive potential surfaces.

4. Discussion

In this section we discuss the 2D-FES and individual fluorescence yields as a function of excitation photon energy in order to obtain the information of potential surfaces of superexcited states and their neutral dissociation dynamics. The dependence of the fluorescence yield on excitation photon energy, i.e., the yield of a particular neutral dissociation channel, reflects the following physical factors: (1) the existence of superexcited states with different excitation probabilities; (2) the features of the crossing between the potential surface of the initial superexcited state and that of dissociative states; (3) the accessibility of dissociative states correlated with different dissociation limits with increasing excitation photon energy.

Factor 1 is the probability for superexcitation at the excitation photon energy of a superexcited state, which can be determined in most cases by the dipole transition amplitude and the Franck−Condon overlap between the ground and superexcited states of N_2O. The initially populated superexcited states lead to the various final products through various decay processes such as the neutral dissociation for fluorescent fragments of which a branching ratio is determined by factor 2 as is seen on the 2D-FES surface. Factor 2 involves the transition probabilities at the crossing ridge between the potential surfaces, which are closely related to the energetic and spatial location of the crossing ridge. Since initially populated superexcited states are distributed to the dissociation limits giving the branching ratios, the opening of another accessible dissociation channel induces an alteration of fluorescence yields, i.e., factor 3.

A. $N_2(a^1\Pi_g)$ Fluorescence. The fluorescence of $N_2(a^1\Pi_g \rightarrow X^1\Sigma_g^+)$ appears in the area between 14.6 and 18.5 eV in the excitation photon energy and between 140 and 200 nm in the fluorescence wavelength as seen in Figure 3. This is the first direct measurement of the molecular fluorescence of the fragment $N_2(a^1\Pi_g)$ state produced in the photodissociation of N_2O.

A threshold-energy electron impact experiment of N_2O[29] obtained the yield of the $N_2(a^1\Pi_g)$ fragment with a threshold at 10.30 eV. The authors concluded that $N_2(a^1\Pi_g)$ was populated via the dissociation of a triplet state of N_2O into $N_2(a^1\Pi_g) + O(^3P)$ with a threshold energy of 10.27 eV.[29] In the present photodissociation experiment, almost no fluorescence of $N_2(a^1\Pi_g \rightarrow X^1\Sigma_g^+)$ appears in the range of the excitation photon energy higher than 20 eV, as seen in Figure 3. This implies the absence of significant dissociation channels of superexcited states of N_2O producing $N_2(a^1\Pi_g)$ in the range higher than 20 eV. This is not in contradiction to ref 29, since the authors reported an almost constant yield of $N_2(a^1\Pi_g)$ at an electron impact energy above 20 eV.

In ref 5 it has been suggested that the photodissociation channel leading to fragments of $N_2(a^1\Pi_g) + O(^1D)$ with a threshold energy of 12.24 eV is the major dissociation channel for producing $N_2(a^1\Pi_g)$ fragments with only a minor contribution from the channel of $N_2(a^1\Pi_g) + O(^3P)$ based on the increase of the fluorescence intensity in the undispersed FES above the threshold energy of $N_2(a^1\Pi_g) + O(^1D)$. However, since the present range of the excitation energy is above the threshold energy of $N_2(a^1\Pi_g) + O(^1D)$, it is difficult to give a conclusive discussion of whether the increase of the fluorescence intensity in ref 5 is due to the opening of the channel of $N_2(a^1\Pi_g) + O(^1D)$ or to other dissociation channels. Concerning the precursor state and the dissociation limit that produce the $N_2(a^1\Pi_g)$ fragment, however, the following three arguments are found with the aid of the 2D-FES measurement to identify the dissociation products to $N_2(a^1\Pi_g) + O(^1D$ or $^1S)$ via the dissociation of precursor singlet superexcited states.

The first argument is that the fluorescence yield of $N_2(a^1\Pi_g \rightarrow X^1\Sigma_g^+)$ shows many peak structures, i.e., the fluorescence yield is enhanced at the excitation photon energies for the

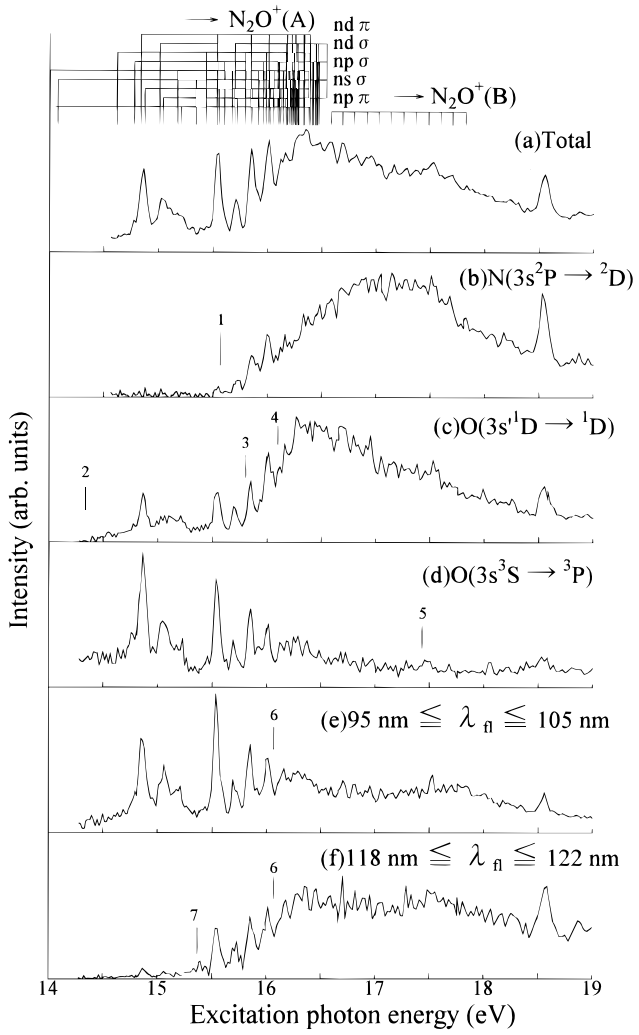

Figure 4. Fluorescence yields as a function of the excitation photon energy: (a) total fluorescence yield in the range of the fluorescence wavelength 80−200 nm; (b) partial fluorescence yield curve of N($3s^2P \rightarrow {}^2D$) at 149.3 nm; (c) that of O($3s'^1D \rightarrow {}^1D$) at 115.2 nm; (d) that of O($3s^3S \rightarrow {}^3P$) at 130.4 nm; (e) that of the fluorescence in the range 95−105 nm, which includes fluorescence lines of O($4s^3S \rightarrow {}^3P$ at 104.1 nm), O($3d^3D \rightarrow {}^3P$ at 102.7 nm), O($3s''^1P \rightarrow {}^1D$ at 99.9 nm), and O($3s'^3D \rightarrow {}^3P$ at 98.8 nm); (f) that of the fluorescence in the range 118−122 nm, which includes fluorescence lines of O($3s''^1P \rightarrow {}^1S$ at 121.8 nm) and N($3s^4P \rightarrow {}^4S$ at 120.0 nm). Assignments of the Rydberg series converging to $N_2O^+(A^2\Sigma^+, B^2\Pi)$ are indicated. The vertical bars indicate the dissociation thresholds as follows: (1) N($3s^2P$) + NO($X^2\Pi$); (2) O($3s'^1D$) + $N_2(X^1\Sigma_g^+)$; (3) O($3p'^1F$) + $N_2(X^1\Sigma_g^+)$; (4) O($3p'^1D$) + $N_2(X^1\Sigma_g^+)$; (5) O($3s^3S$) + $N_2(A^3\Sigma_u^+)$; (6) O($3s''^1P$) + $N_2(X^1\Sigma_g^+)$; (7) N($3s^4P$) + NO($X^2\Pi$).

Rydberg states in Figure 3. Since the ground state of N_2O is the singlet state, the precursor states of neutral dissociation are singlet Rydberg states.

The second argument is derived from other features. According to the intensity distribution of the $N_2(a^1\Pi_g)$ fluorescence on the 2D-FES in Figure 3, one can notice that the shortest wavelength of the fluorescence becomes shorter with increasing excitation photon energy from 14 to about 17 eV. This can be interpreted as a change of the vibrational distribution in the $N_2(a^1\Pi_g)$ excited state when the available energy is increased. From the potential curves for $N_2(a^1\Pi_g)$ and $N_2(X^1\Sigma_g^+)$,[30] the increase of the vibrational energy of $N_2(a^1\Pi_g)$ causes the inner turning-point to move to shorter internuclear distances, thus producing fluorescence at shorter wavelengths, while the outer turning-point is caused to move to longer internuclear distances, producing fluorescence at wavelengths longer than 200 nm, which is not detectable in this experiment. Since it is likely that an increase of the excitation photon energy gives higher vibrational levels of $N_2(a^1\Pi_g)$ fragments, the shortest wavelength edge of the $N_2(a^1\Pi_g)$ fluorescence becomes shorter with increasing excitation photon energy.

The third argument is as follows. The $N_2(a^1\Pi_g \rightarrow X^1\Sigma_g^+)$ fluorescence is vanishingly weak in the excitation photon energy above about 20 eV. This can be rationalized if we assume that the $N_2(a^1\Pi_g)$ is no longer produced in a vibrational bound state but in a vibrational continuum in this photon energy range, i.e., three-body dissociation. Since the threshold energies for the dissociation into $N_2(a^1\Pi_g)$ + O(^{3}P), $N_2(a^1\Pi_g)$ + O(^{1}D), and $N_2(a^1\Pi_g)$ + O(^{1}S) are 10.27, 12.24, and 14.45 eV, respectively, the thresholds for three-body dissociation are 16.13, 18.15, and 20.36 eV for N(^{2}D) + N(^{2}D) + O(^{3}P), N(^{2}D) + N(^{2}D) + O(^{1}D), and N(^{2}D) + N(^{2}D) + O(^{1}S), respectively. The threshold energies for the three-body neutral dissociation into N(^{2}D) + N(^{2}D) + O(^{1}D) and N(^{2}D) + N(^{2}D) + O(^{1}S) coincide approximately with the excitation photon energy for the vanishing of the $N_2(a^1\Pi_g \rightarrow X^1\Sigma_g^+)$ fluorescence on the 2D-FES surface, whereas the $N_2(a^1\Pi_g)$ fluorescence is still strong even at the threshold energy for neutral dissociation into N(^{2}D) + N(^{2}D) + O(^{3}P). The vanishing of the $N_2(a^1\Pi_g)$ fluorescence at about 20 eV thus indicates the switch from a two-body neutral dissociation into $N_2(a^1\Pi_g)$ + O(^{1}D or ^{1}S) to a three-body neutral dissociation into N(^{2}D) + N(^{2}D) + O(^{1}D or ^{1}S). This corresponds to the first argument because $N_2(a^1\Pi_g)$ and O(^{1}D or ^{1}S) build up a singlet state. Furthermore, the third argument is a natural analogy of the second argument for the production of higher vibrational states of the $N_2(a^1\Pi_g)$ fragment, which allows us to predict the following potential surface and the three-body dynamics on the surface. It is supposed that the bottom of the potential well on the surface most likely converges to the well of the $N_2(a^1\Pi_g)$ state and that the potential surface in the Franck−Condon area from the ground-state N_2O is repulsive for the direction of N_2−O bond dissociation and corresponds to a much steeper inner repulsive wall for the N−NO bond. The precursor superexcited states excited in the Franck−Condon area thus starts "symmetric stretching" dissociation with a higher energy of N−NO motion than that of N_2−O. However, below the threshold energy of three-body neutral dissociation, only the dissociation into $N_2(a^1\Pi_g)$ + O is accessible. The three-body dissociation is prohibited by the repelling force at the outer potential wall for the N−NO bond on the potential surface. This induces an energetic backward motion of N−NO with a large amplitude vibration, which provides most of the kinetic energy released into the vibrational energy of $N_2(a^1\Pi_g)$. The rest of the small fraction is given for the relative dissociation energy of $N_2(a^1\Pi_g)$ + O. Above the threshold energy of three-body dissociation the energy of N−NO stretch exceeds the potential energy of the outer wall and "symmetric stretching" three-body dissociation is made possible.

As a conclusion, the $N_2(a^1\Pi_g)$ fluorescence is due to the dissociation of precursor singlet superexcited states to $N_2(a^1\Pi_g)$ + O(^{1}D or ^{1}S).

B. Excitation Photon Energy Range 14.3−18.2 eV. Since the lowest threshold energy for dissociative ionization excitation resulting in the emission of vacuum ultraviolet radiation detectable in the present experiment is, as mentioned above, 23.89 eV, all fluorescence lines and bands originate from neutral dissociation fragments below this energy. In the excitation photon energy range 14.3−18.2 eV, Rydberg series that converge to $N_2O^+(A^2\Sigma^+$ at IP = 16.38 eV) and $N_2O^+(B^2\Pi$ at IP = 18.23 eV) exist.[5,8,9,11,15] Rydberg states that belong to a series converging to $N_2O^+(A^2\Sigma^+)$ are enhanced, which are shown as horizontal structures in the 2D-FES.

The fluorescence yields as a function of the excitation energy are different from each other depending on the fragment species. For example, the fluorescence lines of O($3s'^1$D) at 115.2 nm and N($3s^2$P) at 149.3 nm are strongly enhanced between 16 and 18 eV whereas the O($3s^3$S) fluorescence at 130.4 nm almost vanishes in the same region of the excitation photon energy. Such features are discussed in detail with the use of Figures 4, since the intensities in Figure 3 are placed on a logarithmic scale.

In ref 5 the FES has been measured for the fluorescence wavelength between 113 and 180 nm and peak structures at the excitation photon energy between 14.3 and 16.3 eV have been assigned as Rydberg series ($nd\pi$, $nd\sigma$, $ns\sigma$, $np\sigma$, $np\pi$) that converge to $N_2O^+(A^2\Sigma^+)$. Among these series, the $nd\pi$ series that converges to the ionic (0,0,0) vibrational state has been shown to have the strongest intensity. The appearance of peaks in the total fluorescence yield in Figure 4a is almost identical with the undispersed FES of ref 5. Thus, the most intense peaks between 14.3 and 16.3 eV in Figure 4 can be assigned unambiguously to the $nd\pi$ series converging to the (0,0,0) vibrational state of $N_2O^+(A^2\Sigma^+)$, although the present resolution of the excitation energy is much poorer than that in ref 5. Small peaks due to the Rydberg series converging to $N_2O^+(B^2\Pi)$ are also seen in Figure 4a.

B.1. Excitation Photon Energy Range 14.3−16.3 eV. In parts b−f of Figure 4, the peaks belonging to the aforementioned Rydberg series are seen, which are caused by the predissociation of these Rydberg states. In this section, we focus our discussion on parts c−e of Figures 4 whereas parts b and f of Figure 4 are shown for reference and are not discussed in detail. Let us discuss the dissociation processes causing the peaks of these Rydberg series from the energetic points of view.

In the O($3s^3S \rightarrow {}^3P$) yield curve in Figure 4d the fluorescence is ascribed to the lowest dissociation process of O($3s^3$S) + $N_2(X^1\Sigma_g^+)$ (a pair of a triplet-excited O atom and a singlet N_2 molecule) of which the threshold energy is 11.18 eV (see Table 1) up to the threshold energy for the second-lowest dissociation process of O($3s^3$S) + $N_2(A^3\Sigma_u^+)$ (the threshold energy is 17.41 eV), which is expressed by the short vertical bar labeled "5" in Figure 4d. The threshold energy for the process of O($3s^3$S) + N(^{4}S) + N(^{4}S) exceeds the present energy region. In Figure 4e, the observed fluorescence includes the lines of O($4s^3S \rightarrow {}^3P$) at 104.1 nm, O($3d^3D \rightarrow {}^3P$) at 102.7 nm, O($3s''^1P \rightarrow {}^1D$) at 99.9 nm, and O($3s'^3D \rightarrow {}^3P$) at 98.8 nm. As presented in Table 1, the lowest dissociation processes producing O($4s^3$S), O($3d^3$D), O($3s''^1$P), and O($3s'^3$D) have their threshold energies at 13.59, 13.75, 16.05, and 14.23 eV, respectively. Since the second-lowest processes of O($4s^3$S) + $N_2(A^3\Sigma_u^+)$, O($3d^3$D) + $N_2(A^3\Sigma_u^+)$, and O($3s'^3$D) + $N_2(A^3\Sigma_u^+)$ have their threshold energies at 19.81, 19.97, and 20.45 eV, respectively, the fluorescence in Figure 4e is ascribed to the lowest dissociation processes of O($4s^3$S) + $N_2(X^1\Sigma_g^+)$, O($3d^3$D) + $N_2(X^1\Sigma_g^+)$, and O($3s'^3$D) + $N_2(X^1\Sigma_g^+)$ up to the threshold energy for the process of O($3s''^1$P) + $N_2(X^1\Sigma_g^+)$ expressed by the vertical bar labeled "6" in Figure 4e. The lowest threshold energies for three-body dissociation producing O($4s^3$S), O($3d^3$D), and O($3s'^3$D) lie higher than 20 eV. These are also the case for a pair of a triplet-excited O atom and a singlet N_2 molecule. Based on the building-up principle[31] on a single potential curve or surface, a pair of singlet and triplet fragments ought to originate from a precursor superexcited N_2O in a triplet state. It is likely that the precursor superexcited states are singlet, since the ground state of N_2O is singlet and it consists of light atoms. In the present predissociation process, a pair of singlet and triplet fragments are, hence, thought to be produced in the course of dissociation, reflecting the spin−orbit coupling at the crossing ridge of potential surfaces between the initial superexcited state and dissociative state. The present observation of neutral dissociation into a pair of singlet and triplet fragments is a result of a spin-forbidden predissociation at a large internuclear coordinate.

The fluorescence yield of O($3s^3$S) in the excitation photon energy between 14.5 and 16.3 eV is quite similar to the fluorescence yields in the regions of the fluorescence wavelength between 185.0 and 300.0 nm and between 330.0 and 600.0 nm.[22] The fluorescence in the range 330.0−600.0 nm was ascribed to $N_2(C^3\Pi_u)$ emission[32] and that in the range 185.0−300.0 nm to NO* fluorescence. Guyon et al.[22] explained peak structures in the spectra by predissociation of Rydberg states to other repulsive potential surfaces. The similarity between the present fluorescence yield of O($3s^3$S) and those in ref 22 indicates that those fluorescent fragments, $N_2(C^3\Pi_u)$ and NO*, are produced via the same repulsive states as those of O($3s^3$S) fragments.

B.2. Excitation Photon Energy Range 15.5−18.2 eV. In Figure 4c the fluorescence yield curve of O($3s'^1$D) shows a sudden rise at about 16 eV. This rise cannot be explained by the opening of dissociation channels into O($3s'^1$D) + N_2, since the lowest dissociation process, O($3s'^1$D) + $N_2(X^1\Sigma_g^+)$, has a threshold energy of 14.41 eV (see Table 1) and the second one, O($3s'^1$D) + $N_2(A^3\Sigma_u^+)$, has a threshold energy of 20.63 eV. A possible explanation for this is the dissociation process of O($3p'^1$F) + $N_2(X^1\Sigma_g^+)$ with a threshold energy of 15.81 eV indicated by the vertical bar labeled "3" and that of O($3p'^1$D) + $N_2(X^1\Sigma_g^+)$ with a threshold energy of 16.14 eV labeled "4", where both O($3p'^1$F) and O($3p'^1$D) decay into O($3s'^1$D).

In parts b and c of Figure 4, there is a broad enhancement of fluorescence yield in the range of the excitation photon energy of 15.5−18.0 eV. A broad but weak structure appears in the same region in parts e and f of Figure 4.

The total dissociation yield, i.e., the difference between the photoabsorption cross section and the photoionization cross section,[32] and the O yield[15] also show a broad structure in the same region of the excitation photon energy. The undispersed FES[5] in the same region shows a broad enhancement in intensity that is attributed to the opening of neutral dissociation into N($3s^2$P) + NO($X^2\Pi$) at 15.62 eV, N($2p^4$ ^{4}P) + NO($X^2\Pi$) at 15.86 eV, and O($3s''^1$P) + $N_2(X^1\Sigma_g^+)$ at 16.05 eV. The present measurement enables us to examine the assignment of the features in the undispersed FES in ref 5 using the partial fluorescence yields in parts b, c, e, and f of Figure 4. The fluorescence yield of N($3s^2P \rightarrow {}^2D$) in Figure 4b shows the predicted threshold at 15.6 eV labeled "1" (see Table 1), which is smoothly followed by the above-mentioned broad enhancement. The N($2p^4$ $^4P \rightarrow {}^4S$) fluorescence at 113.4 nm is, however, almost absent in the present measurement. Although the O($3s''^1P \rightarrow {}^1D$ and ^1S) fluorescence at 99.9 and 121.8 nm, respectively (see Table 1), is involved in the detection region of fluorescence in parts e and f of Figures 4, respectively, only a weak threshold at 16.05 eV labeled "6" corresponding to the formation of O($3s''^1$P) and a weak broad enhancement in the region between 16 and 18 eV are observed. The shape of the broad enhancement in Figure 4c is quite similar to that of the total fluorescence yield in Figure 4a. The contribution of the O($3s'^1D \rightarrow {}^1D$) fluorescence to the broad enhancement in Figure 4a, therefore, seems to be large, although the contribution was ignored in ref 5. On the basis of the above discussion, it is concluded that the broad enhancement seen in Figure 4a and ref 5 is attributed to the N($3s^2P \rightarrow {}^2D$) fluorescence yield in Figure 4b and the O($3s'^1D \rightarrow {}^1D$) fluorescence yield in Figure 4c. It must be also pointed out that since in Figure 3 the $N_2(a^1\Pi_g \rightarrow X^1\Sigma_g^+)$ fluorescence shows a broad enhancement in the range of the excitation photon energy 16−18 eV, the

contribution of the $N_2(a^1\Pi_g \rightarrow X^1\Sigma_g^+)$ fluorescence to the broad enhancement in Figure 4a does not seem negligible.

The present observation implies that there must be repulsive potential surfaces that correlate with $N(3s^2P) + NO(X^2\Pi)$ and $O(3p'^1F$ and $3p'^1D) + N_2(X^1\Sigma_g^+)$. The difference in the shape of the broad structure between the two fluorescence yields in parts b and c of Figure 4 indicates that there are at least two repulsive states in this region.

It should be stressed that only parts b and c of Figures 4 show the broad continuum. The accessible neutral dissociation pairs of $N(3s^2P) + NO(X^2\Pi)$, $O(3p'^1F) + N_2(X^1\Sigma_g^+)$, and $O(3p'^1D) + N_2(X^1\Sigma_g^+)$ for fluorescence in parts b and c of Figure 4 can build up the singlet precursor states of superexcited N_2O. As was described in section B.1, the $O(3s^3S \rightarrow {}^3P)$ fluorescence in Figure 4d is ascribed to the process of $O(3s^3S) + N_2(X^1\Sigma_g^+)$ in the excitation photon energy region below 17.41 eV (vertical bar "5"), where the broad enhancement is not observed. It is thus suggested that the optically allowed repulsive states with singlet spin multiplicity exist in this region, which interact with singlet states but not with triplet states. The results of this spin-allowed dissociation and a spin-forbidden predissociation in section B.1 show that the singlet precursor states discussed in section B.1 can interact with states with triplet spin-multiplicity, though the repulsive states discussed in this section do not. This reflects the strength of the spin−orbit coupling in these states.

In the region between 16.3 and 17.7 eV, weak peak structures are seen in Figure 4a. These structures are due to the Rydberg states converging to $N_2O^+(B^2\Pi)$. It was suggested that these Rydberg states preferentially predissociate into neutral pairs and ion pairs rather than autoionize[5] because of the common appearance of the peaks in the yield curves of vacuum ultraviolet fluorescence,[5] of O^- (ion-pair formation)[15] and O^+,[11] which was concluded to be ascribed to the autoionization of O fragment atoms following neutral dissociation[5] and from the general absence in other ion yields in this energy region. The peaks due to the Rydberg states observed in the present total fluorescence yield in Figure 4a are very weak. They are almost not seen in the partial fluorescence yield curves in parts b−f of Figure 4 because of the low signal-to-noise ratio. This implies that the peaks in Figure 4a do not seem to be due to the excitation of a single fragment by one neutral dissociation process but are due to the summation of various fragments populated by a multistep predissociation. It is likely that the multistep predissociation of these Rydberg states occurs via the interaction with the above-mentioned repulsive singlet states as the first common step, interacting then with other dissociative states to form various fragments.

The autoionization as well as fluorescence is possible for some of these excited fragments.[33] The fluorescence from the autoionizing $O(3s''^1P)$ atoms, i.e., 99.9 and 121.8 nm fluorescence corresponding to the transitions to ^1D and ^1S states, respectively, has been observed as in the case of O_2[6] where the autoionization of the $O(3s''^1P)$ state has also been observed.[34] The fluorescence of $O(3s''^1P \rightarrow {}^1D$ or $^1S)$ is seen in parts e and f of Figure 4 as small peaks due to the Rydberg states converging to $N_2O^+(B^2\Pi)$ on top of a flat continuum in the region between 16.3 and 17.7 eV. This structure is ascribed to the opening of the dissociation channel into $O(3s''^1P) + N_2(X^1\Sigma_g^+)$ with the threshold energy of 16.05 eV (see Table 1 and the vertical bar "6" in parts e and f of Figure 4), which is in agreement with the O^+ ion yield[11] as the result of autoionization of $O(3s''^1P)$ as indicated in ref 5.

As the fluorescence from autoionizing fragment, the fluorescence of $O(3s''^3P \rightarrow {}^3P)$ at 87.7 nm was clearly observed in the measurement of O_2 dissociation.[6] However, the fluorescence of $O(3s''^3P \rightarrow {}^3P)$ is absent as seen in the 2D-FES so that $O(3s''^3P)$ atoms are not produced by photodissociation of N_2O. In this excitation photon energy region, the only accessible neutral dissociation channel for an $O(3s''^3P)$ fragment is $O(3s''^3P) + N_2(X^1\Sigma_g^+)$ for which the threshold energy is 15.81 eV. Thus, the precursor singlet Rydberg states converging to the $N_2O^+(B^2\Pi)$ state interact with the singlet repulsive states responsible for the broad enhancement in parts a−c of Figure 4 to give a pair of $O(3s''^1P) + N_2(X^1\Sigma_g^+)$ as well as $N(3s^2P) + NO(X^2\Pi)$ and $O(3p'^1F$ and $3p'^1D) + N_2(X^1\Sigma_g^+)$ whereas they do not interact with the triplet states resulting in a pair of $O(3s''^3P) + N_2(X^1\Sigma_g^+)$. This also means that the origin of the broad enhancement in parts e and f of Figure 4 is the same as that in parts a−c, although the autoionization of $O(3s''^1P)$ suppresses the extent of the enhancement in parts e and f.

C. Excitation Photon Energy Range 18.2−20.5 eV. Figure 5 shows an expanded view of the 2D-FES in Figure 3 in the excitation photon energy range 18.2−20.5 eV and the fluorescence wavelength range 80−138 nm together with the total fluorescence yield curve. In this region vibronic levels of the five Rydberg series converging to the $N_2O^+(C^2\Sigma^+)$ state were obtained previously by different experiments[5,8,11,15] as shown in the left portion of Figure 5. Although the present bandwidth of the excitation photon energy is too broad to assign peak structures to vibronic levels unambiguously, the total fluorescence yield curve in Figure 5 is essentially the same as the undispersed FES[5] where peak structures were clearly assigned to the $nd\pi$ series owing to the better resolution of the excitation photon energy than the resolution of this experiment. Sharp peak structures in the present total fluorescence yield curve are thus identified as the $nd\pi$ series following ref 5.

In the 2D-FES of Figures 3 and 5, simultaneous enhancement of various fluorescence lines is observed for the $nd\pi$ series, which gives rise to the pronounced horizontal structure on the 2D-FES surfaces. Higher members of the $nd\pi$ Rydberg series ($n \geq 5$) overlap with each other and make a manifold of peaks in the region between 19.5 and 20.0 eV. The fluorescence lines approximately at 89, 106, and 119 nm appear intensely only in this energy region of the excitation photon and are negligibly weak in other regions. The candidates for the origin of these lines are listed in Table 2. It should be noticed that all these fluorescence lines are identified as those originating from $N^*(5d^sL)$ atoms (s is the spin multiplicity, and L is the total orbital angular momentum quantum number). Since the lowest excited state of NO, $a^4\Pi$, lying higher than $NO(X^2\Pi)$ by 4.7 eV, is not accessible energetically as the dissociation partner of $N^*(5d^sL)$ in this energy region of the excitation photon, the present result indicates an enhancement of neutral dissociation into $N^*(5d^sL) + NO(X^2\Pi)$ via the $nd\pi$ Rydberg states converging to the $N_2O^+(C^2\Sigma^+)$. This seems to show an interesting agreement between the orbital angular momentum quantum number of the Rydberg electron in the precursor superexcited N_2O molecules and that in N*produced by their dissociation. This also seems to indicate a particular enhancement of N−N bond dissociation of N_2O Rydberg states converging to the $N_2O^+(C^2\Sigma^+)$ state. It should be noted that in the case of the $N_2O^+(C^2\Sigma^+)$ dissociation the N−N bond dissociation occurs preferentially with about an 80% branching ratio.[11,18] These are in accord with the model that, since a highly excited Rydberg molecule can be regarded as that consisting of an ion core and a weakly interacting Rydberg electron, the dissociation of such a molecule takes a similar path on a similar potential surface to those of the ion core (so-called the core ion model).[35,36] The quantum defect for the $nd\pi$ Rydberg orbital in the series converging to the $N_2O^+(C^2\Sigma^+)$ state is 0.0[11], which means that the Rydberg electron does not penetrate into the ion core much.

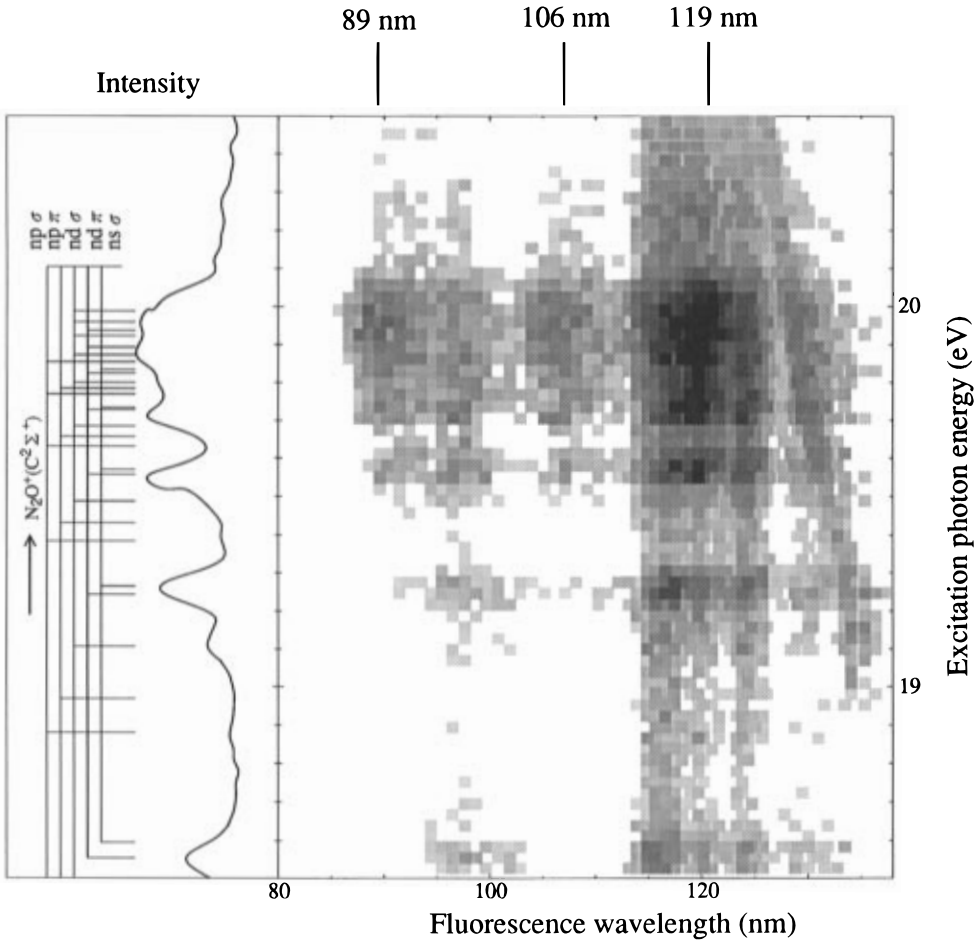

Figure 5. Two-dimensional fluorescence excitation spectrum (2D-FES) in the range of the excitation photon energy 18.23−20.66 eV and the fluorescence wavelength 80−138 nm. This figure is an expanded view of Figure 3. The fluorescence intensity increases exponentially from light to dark. The total fluorescence yield curve plotted on a linear scale and the Rydberg series converging to $N_2O^+(C^2\Sigma^+)$ are also shown in the left portion of the figure.

TABLE 2: Candidates for the Origin of the Enhanced Fluorescence Lines at Approximately 89, 106, and 119 nm in Figure 5[a]

fragment	transition	fluorescence wavelength [nm]	lowest dissociation process	threshold energy [eV]
$N(5d^2D_{5/2})$	$5d^2D_{5/2} \rightarrow {}^4S_{3/2}$	88.53	$N(5d^2D) + NO(X^2\Pi)$	18.93
$N(5d^4P_{5/2})$	$5d^4P_{5/2} \rightarrow {}^4S_{3/2}$	88.57	$N(5d^4P) + NO(X^2\Pi)$	18.93
$N(5d^4P_{3/2})$	$5d^4P_{3/2} \rightarrow {}^4S_{3/2}$	88.59	$N(5d^4P) + NO(X^2\Pi)$	18.93
$N(5d^4D_{5/2})$	$5d^4D_{5/2} \rightarrow {}^4S_{3/2}$	88.63	$N(5d^4D) + NO(X^2\Pi)$	18.92
$N(5d^4F_{5/2})$	$5d^4F_{5/2} \rightarrow {}^4S_{3/2}$	88.68	$N(5d^4F) + NO(X^2\Pi)$	18.91
$N(5d^4F_{3/2})$	$5d^4F_{3/2} \rightarrow {}^4S_{3/2}$	88.70	$N(5d^4F) + NO(X^2\Pi)$	18.91
$N(5d^2D_{5/2,3/2})$	$5d^2D_{5/2,3/2} \rightarrow {}^2D^0_{5/2}$	106.70	$N(5d^2D) + NO(X^2\Pi)$	18.93
$N(5d^4P_{5/2,3/2})$	$5d^4P_{5/2,3/2} \rightarrow {}^2D^0_{3/2}$	106.73	$N(5d^4P) + NO(X^2\Pi)$	18.93
$N(5d^2F_{7/2})$	$5d^2F_{7/2} \rightarrow {}^2D^0_{5/2}$	106.76	$N(5d^2F) + NO(X^2\Pi)$	18.93
$N(5d^4F_{5/2})$	$5d^4F_{5/2} \rightarrow {}^2D^0_{5/2}$	106.85	$N(5d^4F) + NO(X^2\Pi)$	18.92
$N(5d^2F_{7/2})$	$5d^2F_{7/2} \rightarrow {}^2D^0_{5/2,3/2}$	106.87	$N(5d^2F) + NO(X^2\Pi)$	18.91
$N(5d^2D_{5/2})$	$5d^2D_{5/2} \rightarrow {}^2P^0_{5/2,3/2}$	118.90	$N(5d^2D) + NO(X^2\Pi)$	18.93
$N(5d^2D_{3/2})$	$5d^4P_{3/2} \rightarrow {}^2P^0_{5/2,3/2}$	118.92	$N(5d^2D) + NO(X^2\Pi)$	18.93
$N(5d^4D_{5/2})$	$5d^4D_{5/2} \rightarrow {}^2P^0_{3/2}$	119.08	$N(5d^4D) + NO(X^2\Pi)$	18.92
$N(5d^2P_{1/2})$	$5d^2P_{1/2} \rightarrow {}^2P^0_{3/2,1/2}$	119.08	$N(5d^2P) + NO(X^2\Pi)$	18.92
$N(5d^2P_{3/2})$	$5d^2P_{3/2} \rightarrow {}^2P^0_{3/2,1/2}$	119.10	$N(5d^2P) + NO(X^2\Pi)$	18.91

[a] The fragments, the transitions, the fluorescence wavelengths, the lowest dissociation processes for the fragments, and corresponding threshold energies are shown. Transitions are identified according to ref 27. Threshold energies are calculated with the constants in refs 27 and 28.

The neutral dissociation of the $nd\pi$ Rydberg series converging to $N_2O^+(C^2\Sigma^+)$ into $N(5d^sL) + NO(X^2\Pi)$ is therefore well interpreted in a way similar to the dissociation of $N_2O^+(C^2\Sigma^+)$ following the core ion model: the $nd\pi$ Rydberg states converging to the $N_2O^+(C^2\Sigma^+)$ state give N fragment atoms with the same orbital angular momentum, i.e., N(5d). A mixing of states among those resulting in the $N^*(5d^sL)$ formation is possible by way of neutral dissociation through the interaction among the closely lying dissociation surfaces leading to $N^*(5d^sL) + NO(X^2\Pi)$ having similar shapes, which gives various N states arising from the 5d configuration.

It should be noted that the core ion model does not work for the neutral dissociation of the Rydberg states converging to the $N_2O^+(A^2\Sigma^+)$ state. This can be seen in the 2D-FES of Figure 3, where intense peak structures or "horizontal lines" due to the $nd\pi$ Rydberg series converging to $N_2O^+(A^2\Sigma^+)$ are seen

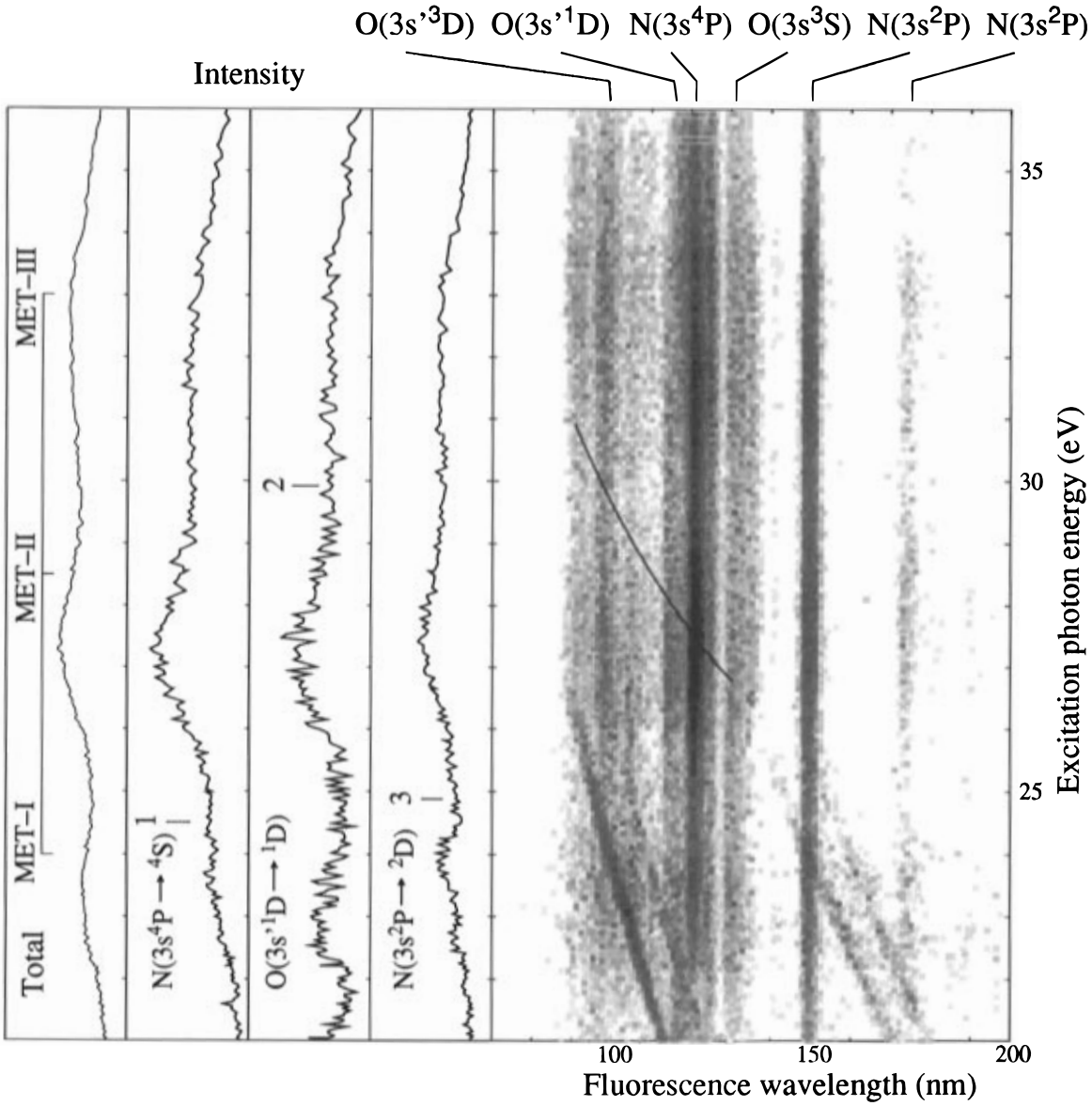

Figure 6. Two-dimensional fluorescence excitation spectrum (2D-FES) in the range of the excitation photon energy 21−36 eV and the fluorescence wavelength 70−200 nm. The fluorescence intensity increases exponentially from light to dark. This figure is an expanded view of Figure 3. The total and partial fluorescence yield curves of $N(3s^4P \rightarrow {}^4S)$, $O(3s'^1D \rightarrow {}^1D)$, and $N(3s^2P \rightarrow {}^2D)$ are also shown in the left portion of the figure. All fluorescence yield curves are on a linear scale. Energies of ionic satellites are indicated in the total fluorescence yield curve. The assignments of the fluorescence lines are indicated at the top of figure. The vertical bars in the partial fluorescence yields indicate dissociation thresholds for the processes (1) $N(3s^4P) + NO^+(X^1\Sigma^+)$, (2) $O(3s'^1D) + N_2^+(X^2\Sigma_g^+)$, and (3) $N(3s^2P) + NO^+(X^1\Sigma^+)$. The curve shows thresholds for the dissociative ionization excitation process resulting in $N_2^+(X^2\Sigma_g^+)$ and O*, which transfers to $O(^3P)$ (see text).

for O* and $N_2(a^1\Pi_g)$ fluorescence. Guyon et al. suggested that this series also produces $N_2(C^3\Pi_u)$ and NO*.[22] These results indicate there is no selective bond dissociation, which cannot be explained by the core ion model, since the dissociation of $N_2O^+(A^2\Sigma^+)$ results in only $N + NO^+$.[18] It seems that this is the result of a slow neutral dissociation due to the weak interaction of the initially populated N_2O Rydberg states with energetically accessible dissociative states, which is in agreement with the result of a small branching ratio into the ionic dissociation of $N_2O^+(A^2\Sigma^+)$.[18] On the other hand, the Rydberg states converging to the $N_2O^+(C^2\Sigma^+)$ state seem to be much more dissociative, since the $N_2O^+(C^2\Sigma^+)$ state has a much more dissociative structure as compared to the $N_2O^+(A^2\Sigma^+)$ state.[18] It should also be pointed out that there is no energetic restriction for neutral dissociation into a connected dissociation limit of N(*n*d) + NO, since the Rydberg states converging to the $N_2O^+(C^2\Sigma^+)$ states are located at higher energies than the threshold for dissociation to N(*n*d) + NO. It is thus supposed that the neutral dissociation of the *n*dπ Rydberg states converging to $N_2O^+(C^2\Sigma^+)$ occurs via a very similar path to the adiabatic dissociation of the ion.

D. Excitation Photon Energy Range above 21 eV. Figure 6 shows the 2D-FES, the total fluorescence yield, and partial fluorescence yields of some fragments in the energy range of the excitation photon above 21 eV. Binding energies of three ionic satellites MET-I, II, and III[17] are shown for reference. The short bars labeled "1", "2", and "3" in partial fluorescence yields indicate the threshold energies of the lowest dissociative ionization excitation (DIE) processes producing each fluorescent fragment (see Table 3). In this energy region, fluorescence from various excited fragments is energetically accessible, which makes it more difficult to interpret the features in the wavelength region of fluorescence between 90 and 140 nm on the 2D-FES surface than those below 20 eV. The assignments of some of these fluorescence lines are shown in Table 3. The strongest of the observed lines corresponds to the transition $N(3s^4P \rightarrow {}^4S)$. This line is very weak in the energy range of the excitation photon below about 20 eV. Other weak fluorescence lines in

TABLE 3: Fluorescent Fragments, Transitions, Fluorescence Wavelengths, Lowest Dissociative Ionization Excitation Processes for the Fragments, and Corresponding Threshold Energies above 20 eV[a]

fragment	transition	fluorescence wavelength [nm]	lowest DIE[b] process	threshold energy [eV]
$N(3s^4P)$	$3s^4P \rightarrow {}^4S$	120.0	$N(3s^4P) + NO^+(X^1\Sigma^+) + e^-$	24.53
$N(3s^2P)$	$3s^2P \rightarrow {}^2D$	149.3	$N(3s^2P) + NO^+(X^1\Sigma+) + e^-$	24.88
$N(3s^2P)$	$3s^2P \rightarrow {}^2P$	174.5	$N(3s^2P) + NO^+(X^1\Sigma+) + e^-$	24.88
$O(3s^3S)$	$3s^3S \rightarrow {}^3P$	130.4	$O(3s^3S) + N_2{}^+(X^2\Sigma_g^+) + e^-$	26.78
$O(3s'^3D)$	$3s'^3D \rightarrow {}^3P$	98.8	$O(3s'^3D) + N_2{}^+(X^2\Sigma_g^+) + e^-$	29.81
$O(3s'^1D)$	$3s'^1D \rightarrow {}^1D$	115.2	$O(3s'^1D) + N_2{}^+(X^2\Sigma_g^+) + e^-$	29.99

[a] Transitions are identified according to ref 27. Threshold energies are calculated with the constants in refs 27 and 28. [b] DIE: dissociative ionization excitation (see text).

TABLE 4: Fluorescent Fragments, Transitions, Fluorescence Wavelengths, Lowest Dissociative Ionization Processes of Three-Body Dissociation, and Those Resulting in the Production of Excited O^+ or N^+, Which Emits Vacuum Ultraviolet Fluorescence in the Range 80−200 nm[a]

fragment	transition	fluorescence wavelength [nm]	lowest DIE[b] process	threshold energy [eV]
$N(3s^4P)$	$3s^4P \rightarrow {}^4S$	120.0	$N(3s^4P) + O^+(^4S) + N(^4S) + e^-$	35.39
$N(3s^4P)$	$3s^4P \rightarrow {}^4S$	120.0	$N(3s^4P) + N^+(^3P) + O(^3P) + e^-$	36.30
$O(3s^3S)$	$3s^3S \rightarrow {}^3P$	130.4	$O(3s^3S) + N^+(^3P) + N(^4S) + e^-$	35.48
$O^+(2p^4\,{}^4P)$	$2p^4\,{}^4P \rightarrow 2p^3\,{}^4S$	83.4	$O^+(2p^4\,{}^4P) + N_2(X^1\Sigma_g^+) + e^-$	30.16
$N^+(2p^3\,{}^3D)$	$2p^3\,{}^3D \rightarrow 2p^2\,{}^3P$	108.4	$N^+(2p^3\,{}^3D) + NO(X^2\Pi) + e^-$	30.90
$N^+(2p^3\,{}^3P)$	$2p^3\,{}^3P \rightarrow 2p^2\,{}^3P$	91.6	$N^+(2p^3\,{}^3P) + NO(X^2\Pi) + e^-$	33.00

[a] Corresponding threshold energies are also shown. Transitions are identified according to ref 27. Threshold energies are calculated with the constants in refs 27 and 28. [b] DIE: dissociative ionization excitation (see text).

this energy range could not be assigned unambiguously because of the many unresolved transition lines.

In the total fluorescence yield in Figure 6, three broad features can be seen with the intensity maxima at the excitation photon energies of about 23, 27.5, and 33 eV, which are in agreement with the undispersed FES of ref 5. The energy dependence of each partial fluorescence yield in the 2D-FES is almost the same as the total fluorescence yield, as seen in the partial fluorescence yields in the left portion of Figure 6. This indicates that each fluorescent fragment has the same precursor molecular states. It is clear that below the lowest threshold energy of the DIE process resulting in the emission of vacuum ultraviolet photon detectable in the present experiment, i.e., 23.89 eV for the process of $O^+(^4S) + N_2(a^1\Pi_g)$, fluorescence on the 2D-FES is ascribed only to neutral dissociation fragments; the broad enhancement of the fluorescence yield at about 23 eV is caused by the neutral dissociation of the precursor superexcited states.

In the energy region above 23.89 eV, there is a possibility that fluorescence is due to DIE processes. Let us identify the dissociation processes responsible for fluorescence in other two broad enhancements. The threshold energy of the DIE process such as $AB \rightarrow A^* + B^+ + e^-$ is written as

$$E_{DIE} = D + IP_B + E_{fl} + E_A + E_{B^+} \qquad (3)$$

where E_{DIE} is the threshold energy for the DIE dissociating into fragments of $A^* + B^+ + e^-$, D the bond dissociation energy of the ground-state molecule AB, IP_B the ionization energy of B, E_{fl} the photon energy of fluorescence of $A^* \rightarrow A + h\nu$, and E_A and E_{B^+} the internal energies of A and B^+, respectively, measured from their ground states. Thus, a linear relation between E_{DIE} and E_{fl} is obtained. This is shown in Figure 6 by a curve corresponding to the DIE processes producing $O^*(nl^sL \rightarrow {}^3P) + N_2{}^+(X^2\Sigma_g^+) + e^-$ using D of 1.68 eV for the $O-N_2$ bond, IP_{N_2} of 15.58 eV, and E_O and $E_{N^2}^+$ of 0 eV.[28] Since the intensity is plotted as a function of the fluorescence wavelength ($\lambda_{fl} = hc/E_{fl}$) and the excitation photon energy in Figure 6, eq 3 gives a curve, not a straight line. We refer to this curve as the "DIE curve". The DIE curve starts at the fluorescence wavelength at 130.4 nm corresponding to $O(3s^3S \rightarrow {}^3P)$ and is terminated at 91.0 nm, which corresponds to the ionization energy of $O(^3P)$, i.e., 13.62 eV, while it traces threshold energies of DIE processes producing $O^*(nl^sL \rightarrow {}^3P)$, $N_2{}^+(X^2\Sigma_g^+)$ and e^-. The fluorescence of $O(nl^sL \rightarrow {}^3P)$ appearing at the excitation photon energies below the DIE curve is attributed to the neutral dissociation of the precursor superexcited states, since the DIE curve traces the lowest threshold energy for the DIE processes producing $O(nl^sL)$ excited states giving fluorescence by the transition to $O(^3P)$.

The lowest DIE threshold producing $O(3s'^3D)$ corresponds to $O(3s'^3D) + N_2{}^+(X^2\Sigma_g^+) + e^-$ and is at 29.81 eV (see Table 3), as indicated by the intersection point of the DIE curve with the vertical line for $O(3s'^3D \rightarrow {}^3P)$ fluorescence at 98.8 nm in Figure 6, below which $O(3s'^3D)$ atoms are produced only by neutral dissociation. The broad feature in the $O(3s'^3D \rightarrow {}^3P)$ fluorescence yield centered at about 27.5 eV is thus due to the neutral dissociation of the precursor superexcited states. The vertical line for the $O(3s'^1D \rightarrow {}^1D)$ fluorescence at 115.2 nm is intersected with the DIE curve at about 28.0 eV. In this case, however, the internal energy of the lower state of fluorescence, $O(^1D)$, is $E_O = 1.97$ eV above $O(^3P)$ so that the exact DIE threshold energy for $O(3s'^1D) + N_2{}^+(X^2\Sigma_g^+) + e^-$ lies 1.97 eV higher than that indicated by the intersecting point. The exact lowest DIE threshold energy is indicated in the partial fluorescence yield of $O(3s'^1D \rightarrow {}^1D)$ by the vertical bar labeled "2" (see Figure 6). Thus, the broad enhancement of the $O(3s'^1D \rightarrow {}^1D)$ fluorescence yield centered at the excitation photon energy of about 27.5 eV is also due to the neutral dissociation of the precursor superexcited states.

We remark that the yields of fluorescence lines in Figure 6 show almost the same dependence on the excitation photon energy as the $O(3s'^3D \rightarrow {}^3P)$ and the $O(3s'^1D \rightarrow {}^1D)$ yield curves. The broad enhancement at the excitation photon energy of about 27.5 eV is generally observed in each fluorescence yield on the 2D-FES. This indicates that each fluorescent fragment causing this broad enhancement is due to the neutral dissociation of the same precursor superexcited states as those causing the broad enhancement in the $O(3s'^3D \rightarrow {}^3P)$ and the $O(3s'^1D \rightarrow {}^1D)$ yield curves. Even the broad enhancement at about 27.5 eV seen for the $O(3s^3S \rightarrow {}^3P)$ fluorescence at 130.4 nm appearing above the intersection point with the DIE curve

is due to the neutral dissociation of superexcited states. This is also the case for the broad enhancement at the same photon energy for $N(3s^4P \rightarrow {}^4S)$ fluorescence at 120.0 nm.

For the broad features centered at about 33 eV in Figure 6 the direct identification of the dissociation process is not possible, since the lowest DIE process producing each fluorescent fragment in the 2D-FES is energetically accessible at the excitation photon energy above 33 eV (see Table 3). The dissociation process for this enhancement can be, however, identified tentatively by use of the results on the branching ratio of the ionic dissociation of MET-I−III.[18] Only the DIE process of $O^+({}^4S) + N_2(a^1\Pi_g) + e^-$ is energetically accessible for the ionic dissociation of MET-I as a DIE process producing fragments that emit vacuum ultraviolet fluorescence at 80−200 nm. The decays of MET-II and MET-III are assigned to the production of O^+ or N^+ with 100% probability.[18] Since no molecular fluorescence including $N_2(a^1\Pi_g)$ fluorescence is observed, there is a possibility that some of the DIE processes in Table 4 contribute to the broad enhancement in the yield curves of the fluorescence lines of atomic nitrogen and oxygen at the excitation photon energy of about 33 eV. However, since the lowest threshold energies for all the three-body DIE processes including those in Table 4 lie above the binding energy of MET-III at 33 eV,[17] the possibility of a contribution from the three-body DIE processes to the broad enhancement at about 33 eV is scarce. Only three DIE processes producing excited O^+ or N^+, which emits vacuum ultraviolet fluorescence in the range 80−200 nm are energetically accessible in this excitation energy range, as seen in Table 4. It seems, however, that fluorescence lines in Figure 6 corresponding to $O^+(2p^4\ {}^4P \rightarrow {}^4S)$ at 83.4 nm, $N^+(2p^3\ {}^3D \rightarrow {}^3P)$ at 108.4 nm, and $N^+(2p^{33}P \rightarrow {}^3P)$ at 91.6 nm do not appear above their threshold energies. The possibility of the contribution from these excited O^+ and N^+ fluorescence lines would thus be negligible in Figure 6. In conclusion, the broad enhancement at the excitation photon energy of about 33 eV is ascribed tentatively to the neutral dissociation of precursor superexcited states.

It should be noted that only broad enhancements with no sharp peaks are seen in Figure 6. The broad enhancements at about 23 and 27 eV are attributable to the neutral dissociation of precursor superexcited states, and that at about 33 eV is also attributable, though tentatively, to the neutral dissociation of precursor superexcited states as discussed above. It indicates that these superexcited states have repulsive potential surfaces. A high-resolution Al Kα X-ray photoelectron spectrum showed rather broad features for the highly excited ions.[37] The precursor superexcited states are thus attributed to multiply excited neutral states having a core configuration of MET ionic satellites or to antibonding valence excited states from the 4σ or 5σ inner-valence orbital.[5] The broad features in the fluorescence yield curves would probably consist of overlapping manifolds of these neutral states.

Many narrower peaks in the yield curve of ion-pair formation have been observed in the excitation photon energy range between 25 and 35 eV, and they have been attributed to Rydberg states converging to MET-II and III.[16] The present energy resolution of the excitation photon (0.19 eV at 30 eV) is poorer than that of their experiment (0.06 eV) but enough to resolve clearly the peaks, if any, since the observed peak width is ∼0.5 eV and the separation is ∼1 eV.[16] In fact, no peak is observed in the present experiment, as seen in Figure 6. Moreover, in the undispersed FES of ref 5 with a resolution of 0.06 eV and better signal-to-noise ratio, those peaks were not observed either. The peaks observed in ref 16 were recorded through the coincidence of O^- and N^+/N_2^+, but they were not pronounced or were absent in the total O^- yield with better signal-to-noise ratio.[15] It is interesting that different results are obtained among the measurements of fluorescence and ion-pair yields. This difference may indicate that the different superexcited states undergo different decay paths.

The increase of the contribution from three-body ion-pair formation was shown.[16] In the present measurement, however, clear evidence of three-body neutral dissociation cannot be extracted from Figure 6. This difference between neutral dissociation and ion-pair formation may be due to superexcited states that are different from each other with access to different decay channels, although it is difficult to give a conclusive discussion at present.

5. Summary

In the present investigation the dispersed fluorescence yields of excited photodissociation fragments of N_2O have been obtained by means of the two-dimensional fluorescence spectroscopy as a function of both the excitation photon energy in the range between 14.28 and 36.36 eV and the fluorescence wavelength in the range between 80 and 200 nm, from which detailed information on the neutral dissociation of superexcited states of N_2O has been obtained. The final dissociation products, dissociation limits, and correlation among neutral dissociation potentials of N_2O have been identified. In most cases of the neutral dissociation of superexcited N_2O formed by photoexcitation below 20 eV, it has been shown that the superexcited states undergo multistep predissociation. The neutral dissociation of the $n d\pi$ Rydberg states converging to $N_2O^+(C^2\Sigma^+)$ has shown different behavior from other Rydberg states. The $n d\pi$ Rydberg states preferentially dissociate into $N^*(5d^sL) + NO(X^2\Pi)$. This has been explained by the dissociative character of the precursor Rydberg states based on the core ion model. The neutral dissociation into $N_2(a^1\Pi_g) + O$ has also been shown to switch to a three-body neutral dissociation. Broad features of the enhanced fluorescence observed in the excitation photon energy range above 20 eV have been identified clearly as due to multiply excited neutral states.

Acknowledgment. The present investigation has been performed under the approval of the Photon Factory Program Advisory Committee for 92-156. The authors thank the staff of the Photon Factory for support. They also thank Dr. A. Ehresmann for fruitful discussion. The financial support from a Grant-in-Aid from the Ministry of Education, Science, Sports, and Culture, Japan is acknowledged.

References and Notes

(1) Hatano, Y. In *Dynamics of Excited Molecules*; Kuchitsu, K., Ed.; Elsevier: Amsterdam, 1994; Chapter 6.

(2) Hatano, Y. In *The Physics of Electronic and Atomic Collisions*; Dubé, L. J., Mitchell, J. B. A., McConkey, J. W., Brion, C. E., Eds.; AIP Press: New York, 1995; pp 67−88.

(3) Ukai, M.; Kameta, K.; Kouchi, N.; Nagano, K.; Hatano, Y.; Tanaka, K. *J. Chem. Phys*. **1992**, *97*, 2835.

(4) Ukai, M.; Kameta, K.; Kouchi, N.; Hatano, Y.; Tanaka, K. *Phys. Rev. A* **1992**, *46*, 7019.

(5) Ukai, M.; Kameta, K.; Machida, S.; Kouchi, N.; Hatano, Y.; Tanaka, K. *J. Chem. Phys.* **1994**, *101*, 5473.

(6) Ukai, M.; Machida, S.; Kameta, K.; Kitajima, M.; Kouchi, N.; Hatano, Y.; Ito, K. *Phys. Rev. Lett*. **1995**, *74*, 239.

(7) Ehresmann, A.; Machida, S.; Ukai, M.; Kameta, K.; Kitajima, M.; Kouchi, N.; Hatano, Y.; Ito, K.; Hayaishi, T. *J. Phys. B: At. Mol. Opt. Phys*. **1995**, *28*, 5283.

(8) Tanaka, Y.; Jursa, A. S.; LeBlanc, F. J. *J. Chem. Phys*. **1960**, *32*, 1205.

(9) Shaw, D. A.; Holland, D. M. P.; MacDonald, M. A.; Hopkirk, A.; Hayes, M. A.; McSweeney, S. M. *Chem. Phys*. **1992**, *163*, 387.

(10) Coppens, P.; Smets, J.; Fishel, M. G.; Drowart, J. *Int. J. Mass Spectrom. Ion Phys*. **1974**, *14*, 57.

(11) Berkowitz, J.; Eland, J. H. D. *J. Chem. Phys*. **1977**, *67*, 2740.

(12) Baer, T.; Guyon, P. M.; Nenner, I.; Tabché-Fouhailé, A.; Botter, R.; Ferreira, L. F. A.; Govers, T. R. *J. Chem. Phys*. **1979**, *70*, 1585.
(13) Poliakoff, E. D.; Ho, M. H.; Leroi, G. E.; White, M. G. *J. Chem. Phys*. **1986**, *85*, 5529.
(14) Locht, R.; Hagenow, G.; Hottmann, K.; Baumgärtel, H. *Chem. Phys*. **1991**, *151*, 137.
(15) Mitsuke, K.; Suzuki, S.; Imamura, T.; Koyano, I. *J. Chem. Phys*. **1990**, *92*, 6556.
(16) Yoshida, H.; Mitsuke, K. *J. Chem. Phys*. **1994**, *100*, 8817.
(17) Brion, C. E.; Tan, K. H. *Chem. Phys*. **1978**, *34*, 141.
(18) Hitchcock, A. P.; Brion, C. E.; van der Wiel, M. J. *Chem. Phys*. **1980**, *45*, 461.
(19) Chan, W. F.; Cooper, G.; Brion, C. E. *Chem. Phys*. **1994**, *180*, 77.
(20) Sroka, W.; Zietz, R. *Z. Naturforsch*., *A* **1973**, *28*, 794.
(21) Lee, L. C.; Carlson, R. W.; Judge, D. L.; Ogawa, M. *J. Phys. B* **1975**, *8*, 977.
(22) Guyon, P. M.; Baer, T.; Nenner, I. *J. Chem. Phys*. **1983**, *78*, 3665.
(23) Braunstein, M.; McKoy, V. *J. Chem. Phys*. **1987**, *87*, 224.
(24) Braunstein, M.; McKoy, V. *J. Chem. Phys*. **1989**, *90*, 1535.
(25) Ito, K.; Morioka, Y.; Ukai, M.; Kouchi, N.; Hatano, Y.; Hayaishi, T. *Rev. Sci. Instrum*. **1995**, *66*, 2119.
(26) Ukai, M.; Kouchi, N.; Kameta, K.; Terazawa, N.; Chikahiro, Y.; Hatano, Y. *Chem. Phys. Lett*. **1992**, *195*, 298.
(27) Striganov, A. R.; Sventitskii, N. S. *Tables of Spectral Lines of Neutral and Ionized Atoms*; Plenum: New York, 1968.
(28) Radzig, A. A.; Smirnov, B. M. *Reference Data on Atoms, Molecules, and Ions*; Springer: Berlin, 1985.
(29) Mason, N. J.; Newell, W. R. *J. Phys. B.* **1989**, *22*, 2297.
(30) Gilmore, F. R. *J. Quant. Spectrosc. Radiat. Transfer* **1965**, *5*, 369.
(31) Herzberg, G. *Electronic Spectra and Electronic Structure of Polyatomic Molecules*; Van Nostrand: New York, 1967.
(32) Cook, G. R.; Metzger, P. H.; Ogawa, M. *J. Opt. Soc. Am*. **1968**, *58*, 129.
(33) Itikawa, Y.; Ichimura, A. *J. Phys. Chem. Ref. Data* **1990**, *19*, 637.
(34) Wills, A. A.; Cafolla, A. A.; Comer, J. *J. Phys. B* **1991**, *24*, 3989.
(35) Freund, R. S. *J. Chem. Phys*. **1971**, *54*, 3125.
(36) Hatano, Y. *Comments At. Mol. Phys*. **1983**, *13*, 259.
(37) Gelius, U. *J. Electron Spectrosc*. **1975**, *5*, 983.